

Article

Correlation and Power Distribution of Intercore Crosstalk Field Components of Polarization-Coupled Weakly Coupled Single-Mode Multicore Fibres

José A. P. Morgado ^{1,*},†,‡ and Adolfo V. T. Cartaxo ^{2,†,‡}¹ ISEC-Lisboa—Instituto Superior de Educação e Ciências de Lisboa, 1049-001 Lisboa, Portugal² ISCTE—Instituto Universitário de Lisboa, 1049-001 Lisboa, Portugal; adolfo.cartaxo@lx.it.pt

* Correspondence: jose.morgado@iseclisboa.pt

† Current address: Instituto de Telecomunicações, Av. Rovisco Pais, 1049-001 Lisboa, Portugal.

‡ These authors contributed equally to this work.

Abstract: The correlation and power distribution of intercore crosstalk (ICXT) field components of weakly coupled multicore fibers (WC-MCFs) are important properties that determine the statistics of the ICXT and ultimately impact the performance of WC-MCF optical communication systems. Using intensive numerical simulation of the coupled mode equations describing ICXT of a single-mode WC-MCF with intracore birefringence and linear propagation, we assess the mean, correlation, and power distribution of the four ICXT field components of unmodulated polarization-coupled homogeneous and quasi-homogeneous WC-MCFs with a single interfering core in a wide range of birefringence conditions and power distribution among the field components at the interfering core input. It is shown that, for homogeneous and quasi-homogeneous WC-MCFs, zero mean uncorrelated ICXT field components with similar power levels are observed for birefringence correlation length and birefringence beat length in the ranges of [0.5 m, 10 m] and [0.1 m, 10 m], respectively, regardless of the distribution of power between the four field components at the interfering core input.

Keywords: birefringence beat length; birefringence correlation length; intercore crosstalk; coupled-mode equations; multicore fiber; polarization-coupled fiber; simulation; weakly coupled



Citation: Morgado, J.A.P.; Cartaxo, A.V.T. Correlation and Power Distribution of Intercore Crosstalk Field Components of Polarization-Coupled Weakly Coupled Single-Mode Multicore Fibres. *Photonics* **2021**, *8*, 191. <https://doi.org/10.3390/photonics8060191>

Received: 10 May 2021
Accepted: 26 May 2021
Published: 29 May 2021

Publisher's Note: MDPI stays neutral with regard to jurisdictional claims in published maps and institutional affiliations.



Copyright: © 2021 by the authors. Licensee MDPI, Basel, Switzerland. This article is an open access article distributed under the terms and conditions of the Creative Commons Attribution (CC BY) license (<https://creativecommons.org/licenses/by/4.0/>).

1. Introduction

Intercore crosstalk (ICXT) is one of the most important physical impairments of weakly coupled multicore fibers (WC-MCFs). The ICXT can limit the use of WC-MCFs in modern optical communication systems (OCSs) by imposing restrictions to the transmission distance [1], core count [2], and use of higher order modulation formats [3]. Nevertheless, WC-MCFs have already been proven as a potential solution to improving the capacity of next-generation OCSs using space division multiplexing [4,5] by increasing their capacities by one order of magnitude comparatively to OCSs using singlecore fibers [5]. In fact, very recently, experiments replicating real-use environments [6,7] and a field-deployed testbed [8] were used to prove the effective potential of WC-MCFs.

In order to devise mitigating strategies for the effects of ICXT on the performance of WC-MCF systems, several works have proposed ICXT models based on coupled-mode theory and coupled-power theory to evaluate the mean ICXT power and other stochastic parameters related to ICXT [9–19]. Relying on those models, the impact of the ICXT on the performance of different types of OCSs were assessed [20–22]. However, although those models have considered effects such as fiber bending, twist, and structure fluctuations in the accumulation of ICXT along the WC-MCF, the impact of birefringence on ICXT accumulation has been much less considered.

WC-MCFs can be classified as follows [23]: (i) polarization-coupled fibers, for which random polarization effects dominate intercore coupling; (ii) scalar-coupled fibers, for

which random structural fiber fluctuations effects dominate intercore coupling; and (iii) mixed-coupled fibers, where both effects, random polarization and random structure fiber fluctuations, are important. Up to now, the majority of studies have considered scalar-coupled WC-MCFs and only a few studies have considered birefringence effects in WC-MCFs [23–26].

In fact, only very recently, it was shown that random polarization-mode coupling due to intracore birefringence can play a crucial role in explaining the ICXT accumulation in polarization-coupled and mixed-coupled WC-MCF [23] and is closely related to the polarization-mode dispersion [26].

The stochastic properties of ICXT power fluctuations have been broadly studied for scalar-coupled WC-MCFs, both theoretically and experimentally. Several studies have considered and others have shown that, for unmodulated homogeneous and quasi-homogeneous WC-MCFs with a single interfering core and multiple interfering cores, under quite general conditions, the four ICXT field components at the WC-MCF output are uncorrelated gaussian components with zero mean and balanced power [11,19,27]. Hence, the ICXT power fluctuations can be modelled by a chi-square (χ^2) distribution with four degrees of freedom [11,19,27].

For polarization-coupled WC-MCFs, a preliminary study of the probability density function (PDF) of the ICXT power fluctuations has been presented [23] where a χ^2 distribution with four degrees of freedom has been shown using numerical simulation for a homogeneous WC-MCF and two pairs of values of birefringence correlation length and birefringence beat length. This shows that, for polarization-coupled WC-MCFs, at least for some specific conditions, the four ICXT field components are zero mean uncorrelated gaussian-distributed. In this context, it is relevant to assess when the mean, the correlation, and the power distribution of the ICXT field components hold those properties under quite general practical conditions of birefringence in polarization-coupled homogeneous and quasi-homogeneous WC-MCFs. This allows us to conclude the validity of modelling the ICXT power fluctuations by a χ^2 distribution with four degrees of freedom in polarization-coupled WC-MCFs.

In this article, the mean, correlation, and power distribution of the ICXT field components in unmodulated polarization-coupled single-mode WC-MCFs are studied by intensive numerical simulation, considering linear propagation and stochastic intracore birefringence effects along a quite large range of birefringence conditions in homogeneous and quasi-homogeneous WC-MCFs. We show that, for both homogeneous and quasi-homogeneous WC-MCFs, the four ICXT field components are zero mean and uncorrelated and have similar power levels for birefringence correlation length and birefringence beat length in the ranges of [0.5 m, 10 m] and [0.1 m, 10 m], respectively.

2. ICXT Model and Computation of Mean ICXT Power in Single-Mode WC-MCFs

This section presents the model used to obtain by numerical simulation the ICXT field of a single-mode WC-MCF considering intracore birefringence and linear propagation. In order to focus the analysis on the statistical properties of the ICXT field generated by each interfering core of a WC-MCF, we consider the interference between two cores only, designated within the paper, generically, by m (interfering core) and n (interfered core).

Figure 1 shows a schematic illustration of the two-core WC-MCF cross section representing the interfering core m (blue) with radius a_m , the interfered core n (red) with radius a_n , the corresponding core pitch Λ_{mn} , and the cladding of the MCF with diameter d_c . The usual range of values for the WC-MCF size parameters are the following: (i) core radius [3.8 μm , 4.7 μm] [17,20,28,29]; (ii) core pitch [30 μm , 45 μm] [8,17,20,28–30]; and (iii) core cladding diameter [125 μm , 260 μm] [5] (p. 22), [8,20,25,29–32].

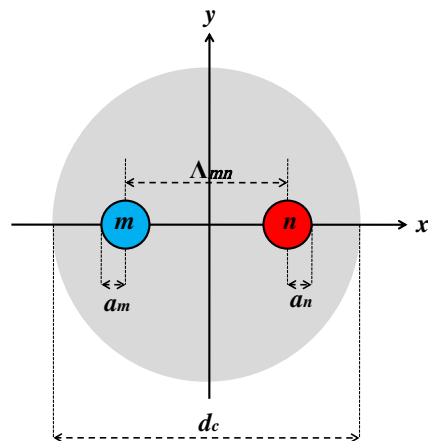


Figure 1. Schematic illustration of a two-core MCF cross section and the cartesian coordinates: core m (interfering core) with radius a_m and core n (interfered core) with radius a_n , the corresponding core pitch Λ_{mn} , and the cladding of the MCF with diameter d_c .

2.1. Evolution of Interfering and Interfered Fields in a Single-Mode WC-MCF

The coupled-mode equations (CME) used to model the crosstalk between cores m and n of a single-mode WC-MCF assuming intracore birefringence and linear propagation along the longitudinal coordinate of the MCF, z , with the propagation constants perturbed by fiber bending and twisting is given by [23]

$$\frac{dE_{n,x}(z)}{dz} = -j\beta'_{c,n}(z) \cdot E_{n,x}(z) - j\frac{\beta_{n,1}(z)}{2} \cdot E_{n,x}(z) - j\frac{\beta_{n,2}(z)}{2} \cdot E_{n,y}(z) - j\kappa'_{nm}(z) \cdot E_{m,x}(z) \quad (1a)$$

$$\frac{dE_{n,y}(z)}{dz} = -j\beta'_{c,n}(z) \cdot E_{n,y}(z) - j\frac{\beta_{n,2}(z)}{2} \cdot E_{n,x}(z) + j\frac{\beta_{n,1}(z)}{2} \cdot E_{n,y}(z) - j\kappa'_{nm}(z) \cdot E_{m,y}(z) \quad (1b)$$

$$\frac{dE_{m,x}(z)}{dz} = -j\beta'_{c,m}(z) \cdot E_{m,x}(z) - j\frac{\beta_{m,1}(z)}{2} \cdot E_{m,x}(z) - j\frac{\beta_{m,2}(z)}{2} \cdot E_{m,y}(z) - j\kappa'_{mn}(z) \cdot E_{n,x}(z) \quad (1c)$$

$$\frac{dE_{m,y}(z)}{dz} = -j\beta'_{c,m}(z) \cdot E_{m,y}(z) - j\frac{\beta_{m,2}(z)}{2} \cdot E_{m,x}(z) + j\frac{\beta_{m,1}(z)}{2} \cdot E_{m,y}(z) - j\kappa'_{mn}(z) \cdot E_{n,y}(z), \quad (1d)$$

where $E_{m,p}(z)$ ($E_{n,p}(z)$) with $p \in \{x, y\}$ is the continuous-wave (CW) polarized fields in core m (n) along the direction p , and $j = \sqrt{-1}$ and $\kappa'_{nm}(z) = \kappa'_{mn}(z) = [\kappa_{mn}(z) + \kappa_{nm}(z)]/2$ with $\kappa_{nm}(z)$ ($\kappa_{mn}(z)$) are the intercore mode-coupling coefficients from core m (n) to core n (m). The average of $\kappa_{mn}(z)$ and $\kappa_{nm}(z)$ is considered in Equation (1) in order to guarantee power conservation at the MCF output [12]. In the following, the index p denotes the polarized field directions x and y , i.e., $p \in \{x, y\}$. For homogeneous MCFs, $\kappa_{nm}(z) = \kappa_{mn}(z)$, and for heterogeneous MCFs, $\kappa_{nm}(z) \neq \kappa_{mn}(z)$; for homogeneous and heterogeneous MCFs, $\kappa'_{nm}(z) = \kappa'_{mn}(z)$. In Equation (1), $\beta'_{c,m}(z)$ and $\beta'_{c,n}(z)$ denote the longitudinal variation of the propagation constants of cores m and n , respectively, which accounts for the fluctuations of the cores effective indexes as well as for the effects of fiber bending and twist. They can be written as [33]

$$\beta'_{c,m}(z) = \beta_{c,m} + \beta_{b,m}(z) \quad ; \quad \beta'_{c,n}(z) = \beta_{c,n} + \beta_{b,n}(z), \quad (2)$$

where $\beta_{c,m} = k_0 \cdot n_{\text{eff},m}^{(\text{int})}$ and $\beta_{c,n} = k_0 \cdot n_{\text{eff},n}^{(\text{int})}$, with $n_{\text{eff},m}^{(\text{int})}$ and $n_{\text{eff},n}^{(\text{int})}$ being the intrinsic effective refractive index of cores m and n , respectively, i.e., the effective refractive index of the cores not perturbed by bend, twist, or any structure fluctuation along the MCF, and $k_0 = 2\pi/\lambda$, where λ is the wavelength. $\beta_{b,m}(z)$ and $\beta_{b,n}(z)$ are the perturbations of the propagation constants induced by bending and twist at the coordinate z of cores m and n , respectively. It should be emphasized that $n_{\text{eff},m}^{(\text{int})}$ and $n_{\text{eff},n}^{(\text{int})}$ are the effective refractive indexes for the fundamental (single) modes propagating through cores m and n , respectively.

The birefringence in cores m and n is modeled by two triplets, $(\beta_{m,1}(z), \beta_{m,2}(z), \beta_{m,3}(z))$ and $(\beta_{n,1}(z), \beta_{n,2}(z), \beta_{n,3}(z))$, respectively [23,34]. It is commonly assumed that, in telecommunication fibers, the circular birefringence is negligible, i.e., $\beta_{n,3}(z) = 0$ ([35], p. 247) and hence, the random modulus model (RMM) with linear birefringence is only adopted in Equation (1) [23,36]. In this case, the first and second components of the birefringence triplets, $\beta_{m,1}(z)$ and $\beta_{m,2}(z)$, and $\beta_{n,1}(z)$ and $\beta_{n,2}(z)$, respectively, are modeled by independent Ornstein–Uhlenbeck random processes while the third components, $\beta_{m,3}(z)$ and $\beta_{n,3}(z)$ are set to zero. In the following, for the sake of notation simplicity, we indicate shortly, $\beta_{m,1}(z)$ and $\beta_{m,2}(z)$ as $\beta_{m,(1,2)}(z)$, and $\beta_{n,1}(z)$ and $\beta_{n,2}(z)$ as $\beta_{n,(1,2)}(z)$. We use this short index notation for other parameters within this article. These random processes are usually characterized by their correlation lengths and beat lengths. In the RMM, the two components of the birefringence, $\beta_{n,(1,2)}(z)$ ($\beta_{m,(1,2)}(z)$), are solutions of the four Langevin equations given by

$$\frac{d\beta_{n,(1,2)}(z)}{dz} = -\rho_n \cdot \beta_{n,(1,2)}(z) + \sigma_n \cdot \eta_{n,(1,2)}(z) \tag{3a}$$

$$\frac{d\beta_{m,(1,2)}(z)}{dz} = -\rho_m \cdot \beta_{m,(1,2)}(z) + \sigma_m \cdot \eta_{m,(1,2)}(z), \tag{3b}$$

where $\eta_{n,(1,2)}(z)$ and $\eta_{m,(1,2)}(z)$ are four independent white gaussian noise sources with zero mean and unitary power spectral density [23,37,38]. Parameters ρ_n and σ_n (ρ_m and σ_m) define the statistical properties of the birefringence in core n (core m). In particular, $\rho_n = 1/L_{C,n}$ ($\rho_m = 1/L_{C,m}$) with $L_{C,n}$ ($L_{C,m}$) as the birefringence correlation length, and $\sigma_n = 2\pi\sqrt{\rho_n}/L_{B,n}$ ($\sigma_m = 2\pi\sqrt{\rho_m}/L_{B,m}$) with $L_{B,n}$ ($L_{B,m}$) as the correlation beat length. The random processes $\beta_{n,1}(z)$ and $\beta_{n,2}(z)$ ($\beta_{m,1}(z)$ and $\beta_{m,2}(z)$) are zero mean Gaussian stationary processes with variances given by $\sigma_n^2/(2\rho_n)$ ($\sigma_m^2/(2\rho_m)$), and their autocorrelation functions are given by [23,36]

$$\mathcal{R}_{\beta_{n,(1,2)}}(z) = \frac{1}{2} \cdot \left(\frac{2\pi}{L_{B,n}}\right)^2 \cdot \exp\left(-\frac{|z|}{L_{C,n}}\right); \mathcal{R}_{\beta_{m,(1,2)}}(z) = \frac{1}{2} \cdot \left(\frac{2\pi}{L_{B,m}}\right)^2 \cdot \exp\left(-\frac{|z|}{L_{C,m}}\right). \tag{4}$$

In the following, we assume that the birefringence vector follows the same statistics in all cores, with $L_B \triangleq L_{B,n} = L_{B,m}$, $L_C \triangleq L_{C,n} = L_{C,m}$ and $\mathcal{R}_\beta(z) \triangleq \mathcal{R}_{\beta_{n,(1,2)}}(z) = \mathcal{R}_{\beta_{m,(1,2)}}(z)$.

The power spectral densities of the exponential autocorrelation functions $\mathcal{R}_{\beta_{n,(1,2)}}(z)$ and $\mathcal{R}_{\beta_{m,(1,2)}}(z)$, represented by $\mathcal{S}_{\beta_{n,(1,2)}}(Y)$ and $\mathcal{S}_{\beta_{m,(1,2)}}(Y)$, respectively, have a Lorentzian shape given by

$$\mathcal{S}_{\beta_{n,(1,2)}}(Y) = \mathcal{S}_{\beta_{m,(1,2)}}(Y) = \left(\frac{2\pi}{L_B}\right)^2 \cdot \frac{L_C}{1 + L_C^2 \cdot Y^2}, \tag{5}$$

where the Fourier transform operator $\mathcal{F}\{\cdot\}$ involving the pair of variables $z \xrightarrow{\mathcal{F}} Y$, defined as

$$G(Y) = \mathcal{F}\{g(z)\} = \int_{-\infty}^{+\infty} g(z) \cdot e^{-jY \cdot z} dz, \tag{6}$$

has been applied to expressions (4) to obtain expression (5).

Defining $\theta_m(z)$ and $\theta_n(z)$ as the accumulated phase due to propagation from the MCF input up to coordinate z in cores m and n , respectively, given by $\theta_m(z) = \int_0^z \beta'_{c,m}(z')dz'$ and $\theta_n(z) = \int_0^z \beta'_{c,n}(z')dz'$, defining

$$A_{n,p}(z) = e^{j\theta_n(z)} \cdot E_{n,p}(z) \quad ; \quad A_{m,p}(z) = e^{j\theta_m(z)} \cdot E_{m,p}(z), \tag{7}$$

and replacing (7) in (1) results in the following CMEs:

$$\begin{aligned} \frac{dA_{n,x}(z)}{dz} = & -j\frac{\beta_{n,1}(z)}{2}A_{n,x}(z) - j\frac{\beta_{n,2}(z)}{2}A_{n,y}(z) - \\ & - j\kappa'_{nm}(z) \cdot e^{-j[\theta_m(z)-\theta_n(z)]} \cdot f_{nm,x}(z) \cdot A_{m,x}(z) \end{aligned} \tag{8a}$$

$$\begin{aligned} \frac{dA_{n,y}(z)}{dz} = & -j\frac{\beta_{n,2}(z)}{2}A_{n,x}(z) + j\frac{\beta_{n,1}(z)}{2}A_{n,y}(z) - \\ & - j\kappa'_{nm}(z) \cdot e^{-j[\theta_m(z)-\theta_n(z)]} \cdot f_{nm,y}(z) \cdot A_{m,y}(z) \end{aligned} \tag{8b}$$

$$\begin{aligned} \frac{dA_{m,x}(z)}{dz} = & -j\frac{\beta_{m,1}(z)}{2}A_{m,x}(z) - j\frac{\beta_{m,2}(z)}{2}A_{m,y}(z) - \\ & - j\kappa'_{mn}(z) \cdot e^{-j[\theta_n(z)-\theta_m(z)]} \cdot f_{mn,x}(z) \cdot A_{n,x}(z) \end{aligned} \tag{8c}$$

$$\begin{aligned} \frac{dA_{m,y}(z)}{dz} = & -j\frac{\beta_{m,2}(z)}{2}A_{m,x}(z) + j\frac{\beta_{m,1}(z)}{2}A_{m,y}(z) - \\ & - j\kappa'_{mn}(z) \cdot e^{-j[\theta_n(z)-\theta_m(z)]} \cdot f_{mn,y}(z) \cdot A_{n,y}(z) \end{aligned} \tag{8d}$$

In the CMEs (8), the terms $f_{nm,p}(z)$ and $f_{mn,p}(z)$ are four random processes introduced to model the phase fluctuations induced locally by the random structure fluctuations along the MCF on the contributions to the field of cores n and m , respectively. These random processes are usually characterized by their correlation lengths. We assume that the processes $f_{nm,p}(z)$ and $f_{mn,p}(z)$ are independent. The influence of this assumption on the ICXT statistics is expected to be reduced. This statement is supported by the fact that, when the birefringence effects can be neglected and the depletion of the interfering field is very low, only the random process that models the phase fluctuation induced on the interfered core affects the ICXT field [18]. Additionally, very small differences in the mean ICXT power estimates obtained by numerical simulation results were observed when independent or equal random processes are considered.

Koshiba et al. analyzed the effects of correlation length of the random process that models the phase fluctuation on the mean ICXT power when that random process includes only the random effect of structure fluctuation and does not include that of macrobend and twist, which are considered deterministic [12,13]. They investigated different types of autocorrelation function of the random process that models the phase fluctuation and found that the exponential autocorrelation function given by

$$\mathcal{R}_f(z) = \exp(-|z|/l_c) \tag{9}$$

is adequate to estimate the mean ICXT power, where l_c is the correlation length of the random process introduced to model the phase fluctuations induced by the random structural fluctuations of the MCF [12,13,33]. In the following, we consider that the random processes $f_{nm,p}(z)$ and $f_{mn,p}(z)$ follow the same statistics, with their autocorrelation functions holding $\mathcal{R}_{f_{nm,p}}(z) = \mathcal{R}_{f_{mn,p}}(z) = \mathcal{R}_f(z)$. The power spectral density corresponding to the exponential autocorrelation function has a Lorentzian shape, and it is given by

$$S_{f_{nm,p}}(Y) = S_{f_{mn,p}}(Y) = \frac{2l_c}{1 + l_c^2 \cdot Y^2} \tag{10}$$

which is obtained by applying the Fourier transform operator defined as (6) to expression (9).

2.2. Computation of the Mean ICXT Power in a WC-MCF

We define the normalized ICXT power, XT , as the ratio between the power at the output of the interfered core n and the power at the input of the interfering core m (with no power launched in core n), i.e.,

$$XT = \frac{|A_n(L)|^2}{|A_m(0)|^2}, \tag{11}$$

where L is the MCF length. The mean of XT is denoted by $\langle XT \rangle$, where $\langle \cdot \rangle$ is the statistical mean operator. In the following, we refer to $\langle XT \rangle$ as the mean ICXT power.

The field in the two directions, x and y , at the interfering core input is described as $A_{m,x}(0) = A_{m,x,I}(0) + jA_{m,x,Q}(0)$ and $A_{m,y}(0) = A_{m,y,I}(0) + jA_{m,y,Q}(0)$, where $A_{m,x,I}(0)$, $A_{m,y,I}(0)$ and $A_{m,x,Q}(0)$, $A_{m,y,Q}(0)$ are the corresponding in-phase (I) and in-quadrature (Q) components. In the following, the index q denotes the quadrature components of the field in direction p , i.e., $q \in \{I, Q\}$. The power distribution at the input of the interfering core m between the two directions x and y , and the two quadrature components, I and Q , is controlled by two parameters, $\zeta_{x,y}$ and $\zeta_{I,Q}$: (i) $\zeta_{x,y} \in [0, 1]$ controls the power distribution between the two directions x and y , and (ii) $\zeta_{I,Q} \in [0, 1]$ controls the power distribution between the I and Q components (assumed the same in both polarization directions). Therefore, the distribution of the field at the input of core m , $A_m(0)$, between the two directions x and y can be written as

$$A_{m,x}(0) = \left\{ (\zeta_{I,Q} \cdot \zeta_{x,y})^{0.5} + j[(1 - \zeta_{I,Q}) \cdot \zeta_{x,y}]^{0.5} \right\} \cdot A_m(0) \tag{12a}$$

$$A_{m,y}(0) = \left\{ \zeta_{I,Q} \cdot (1 - \zeta_{x,y})^{0.5} + j[(1 - \zeta_{I,Q}) \cdot (1 - \zeta_{x,y})]^{0.5} \right\} \cdot A_m(0). \tag{12b}$$

The ICXT field in the two directions at the interfered core output is described as $A_{n,x}(L) = A_{n,x,I}(L) + jA_{n,x,Q}(L)$ and $A_{n,y}(L) = A_{n,y,I}(L) + jA_{n,y,Q}(L)$. The mean ICXT power can be written as

$$\langle XT \rangle = \langle XT_{x,I} \rangle + \langle XT_{x,Q} \rangle + \langle XT_{y,I} \rangle + \langle XT_{y,Q} \rangle, \tag{13}$$

where $XT_{p,q}$ is the ICXT power component that describes the normalized portion of the crosstalk power at the output of the interfered core n in the q component of the p direction of the field, $A_{n,p,q}^2(L)$, with the mean of the ICXT power component given by

$$\langle XT_{p,q} \rangle = \left\langle \frac{A_{n,p,q}^2(L)}{|A_m(0)|^2} \right\rangle. \tag{14}$$

WC-MCFs can be classified in terms of the dominant crosstalk mechanism as follows [23]: (i) *polarization-coupled* fibers, for which $\text{Re}\{\mathcal{R}_\beta^2(z)\}$ is much narrower than $\mathcal{R}_f(z)$, where $\text{Re}\{\cdot\}$ denotes the real part operator; (ii) *scalar-coupled* fibers, for which $\text{Re}\{\mathcal{R}_\beta^2(z)\}$ is much wider than $\mathcal{R}_f(z)$; and (iii) *mixed-coupled* fibers, for which $\text{Re}\{\mathcal{R}_\beta^2(z)\}$ and $\mathcal{R}_f(z)$ are similar widths.

The expressions were derived to assess the mean ICXT power at a generic propagation distance, z , for the following regimes [23]: (i) birefringence correlation length much lower than the birefringence beat length ($L_C \ll L_B$); (ii) birefringence correlation length comparable with the birefringence beat length ($L_C \approx L_B$); and (iii) birefringence correlation length much larger than the birefringence beat length ($L_C \gg L_B$). These are general expressions that can be particularized for polarization-coupled, scalar-coupled, and mixed-coupled fibers. In this article, we consider polarization-coupled WC-MCFs, imposing $l_c \gg L_B, L_C$.

3. Description of the Numerical Simulator and Assessment of the Number of Samples Required to Obtain Stabilized Estimates of the Mean ICXT Power

The objectives of this section are the following: (i) to describe the implementation of the numerical simulator and to discriminate the range of values considered for its parameters, and (ii) to assess the number of samples necessary to obtain stabilized estimates of the mean ICXT power and its four components using the simulator.

3.1. Brief Description about the Simulator Implementation

Four independent random processes $\beta_{n,(1,2)}(z)$ and $\beta_{m,(1,2)}(z)$ with exponential autocorrelation functions given by expressions (4) are generated by solving the stochastic differential Equation (3) using the numerical method proposed in Reference [39], which is a third-order Runge–Kutta method adapted to solve this type of stochastic differential equations. The statistical accuracy of the simulated random processes $\beta_{n,(1,2)}(z)$ and $\beta_{m,(1,2)}(z)$ was confirmed by comparing their autocorrelation and power spectral density functions obtained by simulation with the theoretical expressions (4) and (5), respectively.

Four independent random processes $f_{nm,p}(z)$ and $f_{mn,p}(z)$ with exponential autocorrelation functions given by expression (9) are also considered. As those random processes model the phase fluctuations induced by the random structure fluctuations [12,33], the random processes $f_{nm,p}(z)$ and $f_{mn,p}(z)$ can be written as $f_{nm,p}(z) = \exp [j \cdot w_{m,p}(z)]$ and $f_{mn,p}(z) = \exp [j \cdot w_{n,p}(z)]$, where $w_{m,p}(z)$ and $w_{n,p}(z)$ are four independent Wiener processes that model the phase fluctuations induced by the random structure fluctuations. In order to obtain the exponential autocorrelation function with correlation length l_c , the four Wiener processes are generated by the numerical integration of zero mean white noise with power spectral density of $2/l_c$ [40] (pp. 71–74). The statistical accuracy of the simulated random processes $f_{nm,p}(z)$ and $f_{mn,p}(z)$ was confirmed by comparing their autocorrelation and power spectral density functions obtained by simulation with the theoretical expressions (9) and (10), respectively.

In the numerical simulation, a fifth-order Runge–Kutta method is used to solve the CMEs (8). Two highlights should be mentioned. (i) The step size Δz used to solve numerically Equation (8) should be judiciously selected in order to simulate both the structure fluctuations and birefringence effects rigorously. On one hand, it should hold $\Delta z \ll 1/|\Delta\beta_{c,mn}|$, with $\Delta\beta_{c,mn} = \beta_{c,m} - \beta_{c,n}$, since for correlation lengths of the random structural fluctuations of the order of 1 mm or higher as usually found in WC-MCFs [13,15,29,33] and non-homogeneous WC-MCFs, the faster variation of the right-hand sides of CMEs (1) results from the complex exponentials of the difference of phases θ_m and θ_n , which is imposed by $\Delta\beta_{c,mn}$. On the other hand, $\Delta z \ll L_C$ and $\Delta z \ll \sqrt{2}L_B/(6\pi)$ should also hold, simultaneously, to rigorously simulate the birefringence effects. (ii) In order to be used in the numerical solving of CMEs (1), samples of four independent random processes $\beta_{n,(1,2)}(z)$ and $\beta_{m,(1,2)}(z)$ and four independent Wiener processes $w_{m,p}(z)$ and $w_{n,p}(z)$ with adequate step sizes in z have to be generated.

The mean ICXT power estimated by numerical simulation was obtained considering two situations: polarization-coupled homogeneous ($\Delta\beta_{c,mn} = 0 \text{ rad} \cdot \text{m}^{-1}$) and quasi-homogeneous ($\Delta\beta_{c,mn} = -701 \text{ rad} \cdot \text{m}^{-1}$) WC-MCF with length of $L = 100 \text{ m}$. $\Delta\beta_{c,mn}$ is adjusted by setting adequately the intrinsic effective refractive index of the core n , $n_{\text{eff},n}^{(\text{int})}$. Pairs for the birefringence correlation length and the birefringence beat length (L_C, L_B) have been tested in the ranges of $0.5 \text{ m} \leq L_C \leq 10 \text{ m}$ and $0.1 \text{ m} \leq L_B \leq 10 \text{ m}$, respectively. These ranges have been settled in order to include the set of values found typical for L_C and L_B in singlecore telecommunication fibers [37,41,42] (p. 6), [35] (pp. 251, 261, 267, 269). To the best of authors' knowledge, measured values of the birefringence correlation length and birefringence beat length have not been reported yet for WC-MCFs.

According to the ranges considered for $\Delta\beta_{c,mn}$, L_C and L_B , Δz in the range of $10^{-5} - 10^{-4} \text{ m}$ was used in all simulations, averaging over 200 MCF realizations, with each realization corresponding to different samples of the eight noise random processes $\beta_{n,(1,2)}(z)$ and $\beta_{m,(1,2)}(z)$, and $w_{n,p}(z)$ and $w_{m,p}(z)$.

Table 1 shows the parameters kept constant in the numerical results. We stress that we considered $l_c = 10^6$ m and that the bending radius and twisting period were adjusted so that the bending and twisting effects on the ICXT field can be neglected.

Table 1. Single-mode WC-MCF parameters kept constant in numerical results.

Parameter	Symbol	Value
Wavelength	λ	1550 nm
Intrinsic effective refractive index of core m	$n_{\text{eff},m}^{(\text{int})}$	1.4418 [16]
Core pitch	Λ_{mn}	30 μm [16]
Cartesian coordinates of core m	(x_m, y_m)	$(-\Lambda_{mn}/2, 0)$
Cartesian coordinates of core n	(x_n, y_n)	$(\Lambda_{mn}/2, 0)$
MCF length	L	100 m

The parameters κ'_{mn} and κ'_{nm} were adjusted to $\kappa'_{mn} = \kappa'_{nm} = 4.5 \times 10^{-5} \text{ m}^{-1}$ and $\kappa'_{mn} = \kappa'_{nm} = 4.5 \times 10^{-2} \text{ m}^{-1}$, according to the homogeneous or quasi-homogeneous regimes, respectively, in order to ensure a mean ICXT power range of about $[-90 \text{ dB}, -50 \text{ dB}]$ in all situations tested.

In order to ensure acceptable computation times to estimate the statistical parameters of the ICXT field components through numerical simulation, the MCF length considered in the simulation study is $L = 100$ m. In fact, to generate $\beta_{n,(1,2)}(z)$ and $\beta_{m,(1,2)}(z)$ by solving the stochastic differential Equation (3), to propagate the random signal through the MCF solving the CMEs (8), and to obtain the ICXT power given by (11), a computational time of about 15 min per MCF realization is necessary. As 200 MCF realizations are required to obtain a confident estimate of the mean ICXT, the previous process must be repeated 200 hundreds of times for each (L_B, L_C) pair, leading to a total time of about 50 h per pair. These computational times are reached, running the simulations in a PC having a CPU Intel Core I9 10900KF with a clock speed of 5.3 GHz, a memory cache of 20 MB, and a RAM of 64 GB. These computational times increase proportionally to the MCF length. Therefore, in practical terms, acceptable computational times are hardly compatible to MCF lengths longer than 100 m.

3.2. Dependence of Estimates of Mean ICXT Power on the Number of Samples

Extended simulation tests were performed in order to assess the number of averaging samples necessary to stabilize the mean ICXT power estimator given by (13). A wide range of situations, considering 13 different pairs of birefringence correlation length and birefringence beat length, (L_C, L_B) , in the ranges indicated in Section 3.1, both for homogeneous ($\Delta\beta_{c,mn} = 0 \text{ rad} \cdot \text{m}^{-1}$) and quasi-homogeneous ($\Delta\beta_{c,mn} = -701 \text{ rad} \cdot \text{m}^{-1}$) single-mode WC-MCFs have been tested. For each pair (L_C, L_B) , different power distributions between the two directions x and y , and I and Q components (assumed the same in both polarization directions) of the interfering core (core m) have been tested by assuming different pairs $(\zeta_{x,y}, \zeta_{I,Q})$, namely, $(0, 0)$, $(0, 0.5)$, $(0, 1)$, $(0.5, 0)$, $(0.5, 0.5)$, $(0.5, 1)$, $(1, 0)$, $(1, 0.5)$, and $(1, 1)$.

Figure 2 shows two paradigmatic examples among the universe of situations tested, illustrating the mean ICXT power estimator given by (13) in dB, i.e., $10 \cdot \log_{10}(\langle XT \rangle)$, as a function of the number of samples, as well as each of the four components of Equation (13), $\langle XT_{p,q} \rangle$ also in dB, i.e., $10 \cdot \log_{10}(\langle XT_{p,q} \rangle)$: (i) Figure 2a considers a homogeneous WC-MCF ($\Delta\beta_{c,mn} = 0 \text{ rad} \cdot \text{m}^{-1}$) with $L_C = 10$ m, $L_B = 1$ m, $\zeta_{x,y} = 0.5$ and $\zeta_{I,Q} = 0.5$, and (ii) Figure 2b considers a quasi-homogeneous WC-MCF ($\Delta\beta_{c,mn} = -701 \text{ rad} \cdot \text{m}^{-1}$) with $L_C = 1$ m, $L_B = 1$ m, $\zeta_{x,y} = 0.5$, and $\zeta_{I,Q} = 1$.

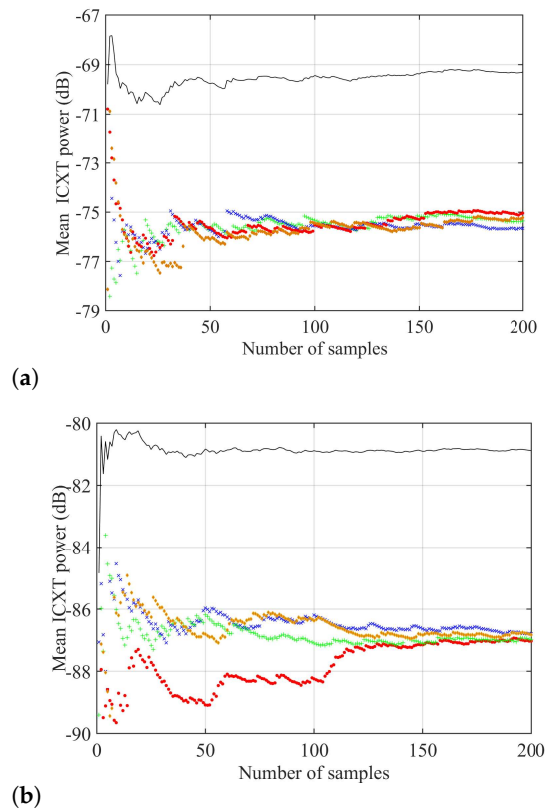


Figure 2. Mean ICXT power in dB at the interfered core output given by (13) and corresponding parcels given by (14) as a function of the number of averaging samples for (a) homogeneous single-mode WC-MCF ($\Delta\beta_{c,mn} = 0 \text{ rad} \cdot \text{m}^{-1}$) with $L_C = 10 \text{ m}$, $L_B = 1 \text{ m}$, $\zeta_{x,y} = 0.5$, and $\zeta_{I,Q} = 0.5$ and (b) quasi-homogeneous single-mode WC-MCF ($\Delta\beta_{c,mn} = -701 \text{ rad} \cdot \text{m}^{-1}$) with $L_C = 1 \text{ m}$, $L_B = 1 \text{ m}$, $\zeta_{x,y} = 0.5$, and $\zeta_{I,Q} = 1$. Continuous line: $\langle XT \rangle$; mark (+): $\langle XT_{x,I} \rangle$; mark (\times): $\langle XT_{x,Q} \rangle$; mark (\bullet): $\langle XT_{y,I} \rangle$; and mark (\blacklozenge): $\langle XT_{y,Q} \rangle$.

Figure 2 shows that the fluctuation of the mean ICXT power estimates occurring for 200 averaging samples is very low and, consequently, the stabilization achieved can be considered adequate. Figure 2 shows also a quasi-uniform distribution between the four components of the mean ICXT power at the interfered core output. Moreover, differences of about 6 dB between the mean ICXT power of each component and the total mean ICXT power are observed, which are in accordance with Equation (13). The fluctuations observed for 200 averaging samples are attributed to the inherent randomness of the estimate of the mean from a finite number of samples.

In the universe of situations tested, the level of fluctuations of the estimate of the mean ICXT power observed with an increase in the number of averaging samples is similar to the one shown in Figure 2. Therefore, all situations tested revealed that 200 averaging samples are adequate to ensure the stabilization of the estimators of mean ICXT power obtained by simulation.

To validate the numerical simulator, several situations were tested to assess the mean ICXT power as a function of L_C for different L_B , namely, 1 m and 10 m, both for homogeneous ($\Delta\beta_{c,mn} = 0 \text{ rad} \cdot \text{m}^{-1}$) and quasi-homogeneous ($\Delta\beta_{c,mn} = -701 \text{ rad} \cdot \text{m}^{-1}$) polarization-coupled WC-MCF. L_C in the range indicated in Section 3.1 was considered. Excellent agreement between simulation estimates and analytical results obtained using the expressions proposed in [23] was achieved in all situations tested.

4. Parameters Used to Characterize the Statistical Properties of the ICXT Field Components

We use the following three parameters to quantify the mean deviation from 0; the level of correlation; and the power unbalancing of the ICXT field components, $A_{n,p,q}(L)$:

(i) The *normalized mean* of the fields components at the WC-MCF output defined by

$$\bar{A}_{n,p,q}(L) = \frac{\langle A_{n,p,q}(L) \rangle}{\sigma_{A_n}}, \quad (15)$$

and σ_{A_n} given by

$$\sigma_{A_n} = \left[\langle [A_{n,x,I}(L) - \langle A_{n,x,I}(L) \rangle]^2 \rangle + \langle [A_{n,x,Q}(L) - \langle A_{n,x,Q}(L) \rangle]^2 \rangle + \langle [A_{n,y,I}(L) - \langle A_{n,y,I}(L) \rangle]^2 \rangle + \langle [A_{n,y,Q}(L) - \langle A_{n,y,Q}(L) \rangle]^2 \rangle \right]^{0.5}, \quad (16)$$

with $-\infty \leq \bar{A}_{n,p,q}(L) \leq +\infty$;

(ii) The *correlation coefficients* of the ICXT field components defined as [43], pp. 153–154.

$$C_{p_1,q_1,p_2,q_2} = \frac{\langle A_{n,p_1,q_1}(L) \cdot A_{n,p_2,q_2}(L) \rangle - \langle A_{n,p_1,q_1}(L) \rangle \cdot \langle A_{n,p_2,q_2}(L) \rangle}{\left(\langle [A_{n,p_1,q_1}(L) - \langle A_{n,p_1,q_1}(L) \rangle]^2 \rangle \right)^{0.5} \cdot \left(\langle [A_{n,p_2,q_2}(L) - \langle A_{n,p_2,q_2}(L) \rangle]^2 \rangle \right)^{0.5}}, \quad (17)$$

with $p_1, p_2 \in \{x, y\}$ and $q_1, q_2 \in \{I, Q\}$ excluding the situations with $(p_1 = p_2 \wedge q_1 = q_2)$. C_{p_1,q_1,p_2,q_2} takes on values in the range $-1 \leq C_{p_1,q_1,p_2,q_2} \leq 1$, with $C_{p_1,q_1,p_2,q_2} = 0$ corresponding to uncorrelated components and with $C_{p_1,q_1,p_2,q_2} = -1$ and $C_{p_1,q_1,p_2,q_2} = 1$ corresponding to fully correlated components.

(iii) The *unbalancing parameter* defined in percentage as

$$\mathcal{U} \triangleq \max_{p,q} \left\{ \left| 4 \frac{\langle XT_{p,q} \rangle}{\langle XT \rangle} - 1 \right| \right\} \times 100\%, \quad (18)$$

with $\langle XT_{p,q} \rangle$ defined as (14), $\langle XT \rangle$ defined as (11), and $\max\{\cdot\}$ defines the maximum of the four values between braces. This parameter assesses the unbalance in the mean power of the four ICXT field components at the WC-MCF output (in the two directions x and y , and in the two quadrature components I and Q). From Equations (13) and (18), we can easily infer the range for \mathcal{U} as $0\% \leq \mathcal{U} \leq 300\%$: (i) when the mean ICXT power is uniformly distributed among the two directions x and y and the two quadrature components I and Q , $\langle XT_{p,q} \rangle = \langle XT \rangle/4$, resulting in $\mathcal{U} = 0\%$; (ii) on the other hand, when the mean ICXT power is entirely in one of the two directions x or y and one of the two quadrature components I or Q , the maximum of the four $\langle XT_{p,q} \rangle$ terms between braces is equal to $\langle XT \rangle$, resulting in $\mathcal{U} = 300\%$.

5. Numerical Results

The objective of this section is, using the simulator developed in Section 3.1, to assess some of the most important statistical properties of the four ICXT field components $A_{n,p,q}(L)$, namely the means, correlations, and unbalancing power between them. Those properties are assessed for a wide range of situations, namely different (L_C, L_B) pairs in the ranges indicated in Section 3.1 and different pairs of $(\zeta_{x,y}, \zeta_{I,Q})$ in the range of $0 \leq \zeta_{x,y} \leq 1$ and $0 \leq \zeta_{I,Q} \leq 1$, both for homogeneous ($\Delta\beta_{c,mm} = 0 \text{ rad} \cdot \text{m}^{-1}$) and quasi-homogeneous ($\Delta\beta_{c,mm} = -701 \text{ rad} \cdot \text{m}^{-1}$) single-mode WC-MCF. More than 200 different situations are tested.

In the following two subsections, we present some of the most representative simulation results achieved considering $L_C = 10 \text{ m}$ and $L_B = 10 \text{ m}$ ($L_C \approx L_B$), $L_C = 1 \text{ m}$

and $L_B = 10\text{ m}$ ($L_C \ll L_B$), and $L_C = 10\text{ m}$ and $L_B = 0.1\text{ m}$ ($L_C \gg L_B$) for homogeneous ($\Delta\beta_{c,mn} = 0\text{ rad}\cdot\text{m}^{-1}$) and quasi-homogeneous ($\Delta\beta_{c,mn} = -701\text{ rad}\cdot\text{m}^{-1}$) single-mode WC-MCF.

5.1. Results for Single-Mode Homogeneous WC-MCF

Figure 3 shows the simulation results of the normalized mean of the $A_{n,x,I}(L)$ field component given by (15) (Figure 3a), the correlation coefficient between the field components $A_{n,x,I}(L)$ and $A_{n,y,Q}(L)$ given by (17) (Figure 3b), and the mean ICXT power of the term $A_{n,x,I}(L)$ given by (14) (in dB) (Figure 3c) for a homogeneous WC-MCF ($\Delta\beta_{c,mn} = 0\text{ rad}\cdot\text{m}^{-1}$) with $L_C = 10\text{ m}$ and $L_B = 10\text{ m}$ (regime $L_C \approx L_B$).

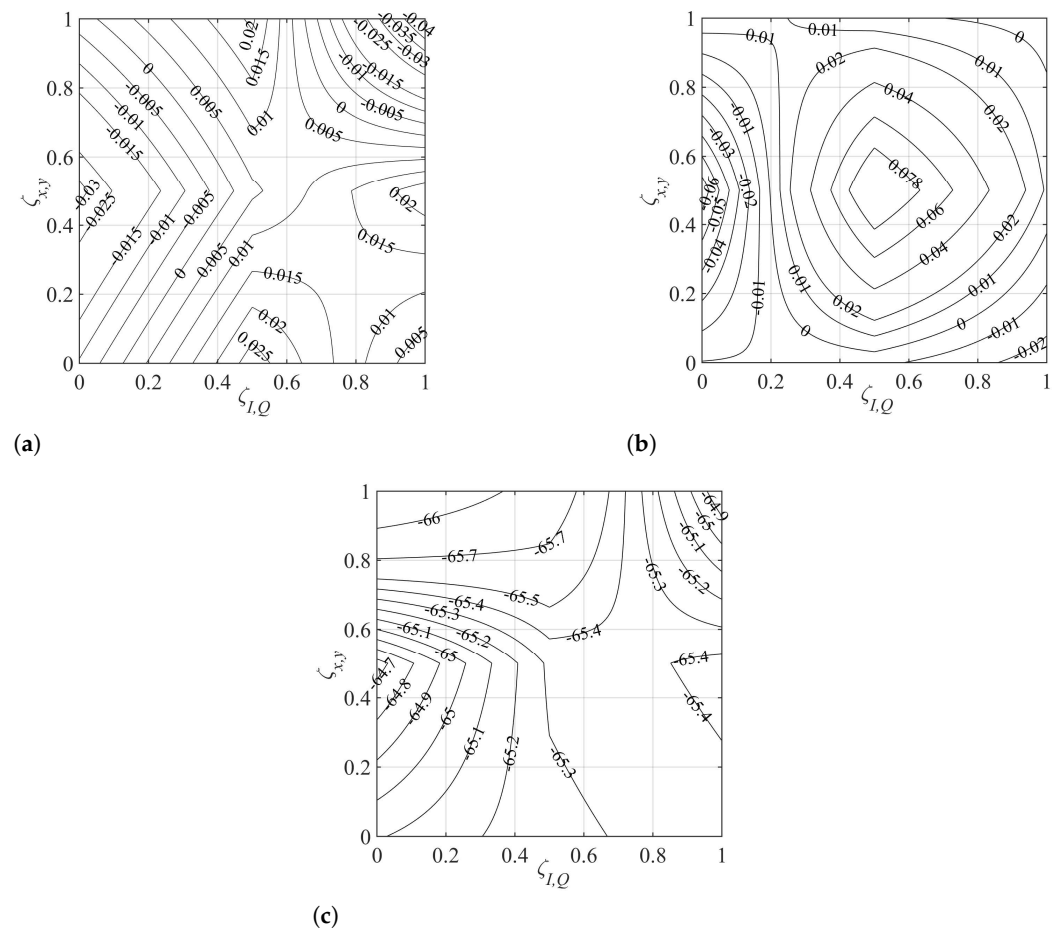


Figure 3. (a) Normalized mean of the I component of the ICXT field in the x direction at the interfered core output; (b) correlation coefficient between the I component of the ICXT field in the x direction and the Q component of the ICXT field in the y direction at the interfered core output; and (c) mean power of the I component of the ICXT field in the x direction at the interfered core output (in dB) for homogeneous WC-MCF ($\Delta\beta_{c,mn} = 0\text{ rad}\cdot\text{m}^{-1}$) with $L_C = 10\text{ m}$ and $L_B = 10\text{ m}$ (regime $L_C \approx L_B$).

Figure 3a shows that the normalized mean of $A_{n,x,I}(L)$ is considerably small in the entire range of power distribution at the interfering core input. Figure 3b shows that a very low correlation between $A_{n,x,I}(L)$ and $A_{n,y,Q}(L)$ is observed regardless of the power distribution at the interfering core input. Figure 3c shows that the mean ICXT power of the term $A_{n,x,I}(L)$ has small variations (lower than 1.5 dB) with the power distribution at the interfering core input. Similar observations hold for the other ICXT field components.

Figure 4 shows the simulation results for the normalized mean of the $A_{n,y,I}(L)$ field component (Figure 4a), the correlation coefficient between the field components $A_{n,y,I}(L)$ and $A_{n,y,Q}(L)$ (Figure 4b), and the mean ICXT power of the term $A_{n,y,I}(L)$ in dB (Figure 4c) with $L_C = 1\text{ m}$ and $L_B = 10\text{ m}$ (regime $L_C \ll L_B$).

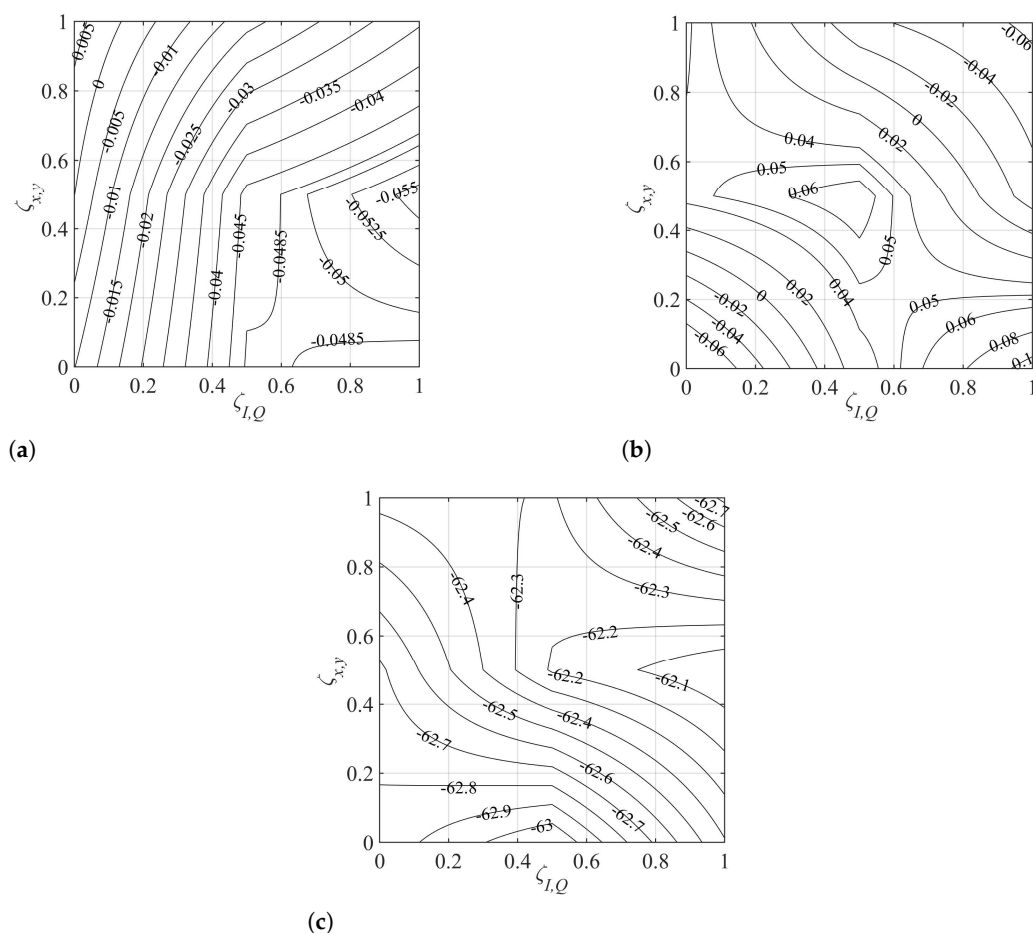


Figure 4. (a) Normalized mean of the I component of the ICXT field in the y direction at the interfered core output; (b) correlation coefficient between the I component of the ICXT field in the y direction and the Q component of the ICXT field in the y direction at the interfered core output; and (c) mean power of the I component of the ICXT field in the y direction at the interfered core output (in dB) for homogeneous WC-MCF ($\Delta\beta_{c,mn} = 0 \text{ rad} \cdot \text{m}^{-1}$) with $L_C = 1 \text{ m}$ and $L_B = 10 \text{ m}$ (regime $L_C \ll L_B$).

Figure 4a shows that the normalized mean of $A_{n,y,I}(L)$ is considerably small in the entire range of power distribution at the interfering core input. Figure 4b shows also that a very low correlation between $A_{n,y,I}(L)$ and $A_{n,y,Q}(L)$ is observed regardless of the power distribution at the interfering core input. Figure 4c shows that the mean ICXT power of the term $A_{n,y,I}(L)$ has small variations (lower than 1 dB) with the power distribution at the interfering core input. Similar observations hold for the other ICXT field components.

In order to analyze the impact of L_B reduction on the variation in the mean, correlation, and mean power of ICXT field components, we maintain $L_C = 10 \text{ m}$ and reduce the beat length to $L_B = 0.1 \text{ m}$. Figure 5 shows the simulation results of the normalized mean of the $A_{n,x,I}(L)$ field component (Figure 5a), the correlation coefficient between the field components $A_{n,x,I}(L)$ and $A_{n,y,I}(L)$ (Figure 5b), and the mean ICXT power of $A_{n,y,Q}(L)$ in dB (Figure 5c) with $L_C = 10 \text{ m}$ and $L_B = 0.1 \text{ m}$ (regime $L_C \gg L_B$). Figure 5a shows that the normalized mean of $A_{n,x,I}(L)$ is considerably small in the whole range of power distribution at the interfering core input. Figure 5b shows a very low correlation between $A_{n,x,I}(L)$ and $A_{n,y,I}(L)$ regardless of the power distribution at the interfering core input. Figure 5c shows that the mean ICXT power of the term $A_{n,y,Q}(L)$ has small variations (lower than 0.7 dB) with the power distribution at the interfering core input. Similar observations hold for the other ICXT field components.

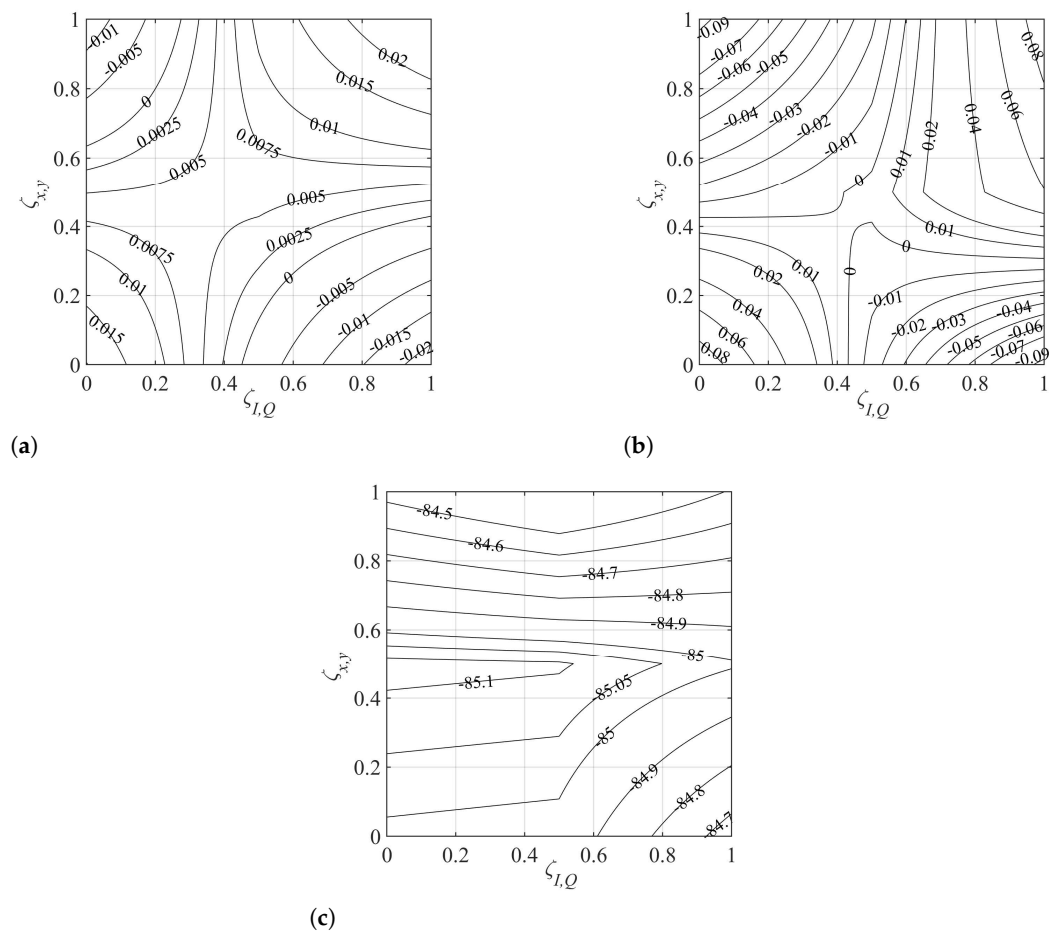


Figure 5. (a) Normalized mean of the I component of the ICXT field in the x direction at the interfered core output; (b) correlation coefficient between the I component of the ICXT field in the x direction and the I component of the ICXT field in the y direction at the interfered core output; and (c) mean power of the Q component of the ICXT field in the y direction at the interfered core output (in dB) for homogeneous WC-MCF ($\Delta\beta_{c,mn} = 0 \text{ rad} \cdot \text{m}^{-1}$) with $L_C = 10 \text{ m}$ and $L_B = 0.1 \text{ m}$ (regime $L_C \gg L_B$).

In order to analyze the dependence of the power unbalance of the four ICXT field components, $A_{n,p,q}(L)$, for homogeneous WC-MCF ($\Delta\beta_{c,mn} = 0 \text{ rad} \cdot \text{m}^{-1}$), on the power distribution at the interfering core input assigned to one of the two directions x or y and one of the two quadrature components I or Q , Figure 6 shows the unbalancing parameter \mathcal{U} for the three previous pairs of values (L_B, L_C) and $\Delta\beta_{c,mn} = 0 \text{ rad} \cdot \text{m}^{-1}$, as a function of $(\zeta_{x,y}, \zeta_{I,Q})$ in the range $0 \leq \zeta_{x,y} \leq 1$ and $0 \leq \zeta_{I,Q} \leq 1$.

Figure 6 shows that values of the \mathcal{U} parameter lower than 20% are achieved for all situations tested. Such a low unbalancing level indicates that a quasi-uniform power distribution between the four components of the ICXT field occurs for homogeneous WC-MCF regardless of the power distribution among the four field components at the interfering core input.

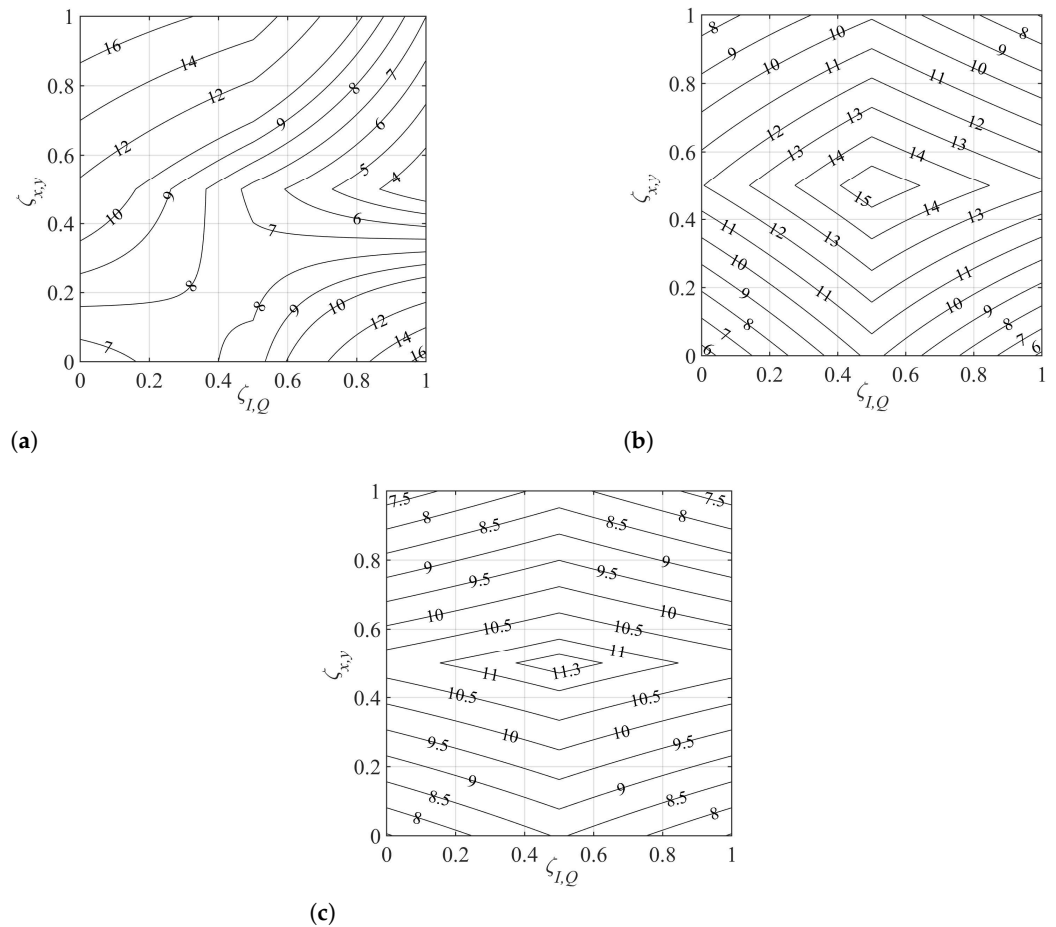


Figure 6. Unbalancing parameter for different pairs (L_B, L_C) and homogeneous WC-MCF ($\Delta\beta_{c,mm} = 0 \text{ rad} \cdot \text{m}^{-1}$): (a) $L_B = 10 \text{ m}$, $L_C = 10 \text{ m}$; (b) $L_B = 10 \text{ m}$, $L_C = 1 \text{ m}$; and (c) $L_B = 0.1 \text{ m}$, $L_C = 10 \text{ m}$.

5.2. Results for Quasi-Homogeneous Single-Mode WC-MCF

In this subsection, we carry out an analysis similar to the one performed in Section 5.1 but for quasi-homogeneous single-mode WC-MCF with $\Delta\beta_{c,mm} = -701 \text{ rad} \cdot \text{m}^{-1}$. We consider the three regimes: (i) $L_C \approx L_B$, (ii) $L_C \ll L_B$, and (iii) $L_C \gg L_B$.

Particularly, for $L_C \approx L_B$, Figure 7 shows the simulation results for the normalized mean of the $A_{n,y,I}(L)$ field component (Figure 7a), the correlation coefficient between the field components $A_{n,y,I}(L)$ and $A_{n,y,Q}(L)$ (Figure 7b), and the mean ICXT power of the term $A_{n,y,I}(L)$ (in dB) (Figure 7c), assuming $L_C = 10 \text{ m}$ and $L_B = 10 \text{ m}$. Similar observations to the ones indicated in Figures 3–5 for homogeneous WC-MCF can be settled from Figure 7. In fact, (i) Figure 7a shows that the normalized mean of $A_{n,y,I}(L)$ is considerably small in the entire range of power distribution at the interfering core input, (ii) Figure 7b shows that a very low correlation between $A_{n,y,I}(L)$ and $A_{n,y,Q}(L)$ is observed regardless of the power distribution at the interfering core input, and (iii) Figure 7c shows that the mean ICXT power of the term $A_{n,y,I}(L)$ has small variations (lower than 0.9 dB) with the power distribution at the interfering core input. Similar conclusions holds for the other field components.

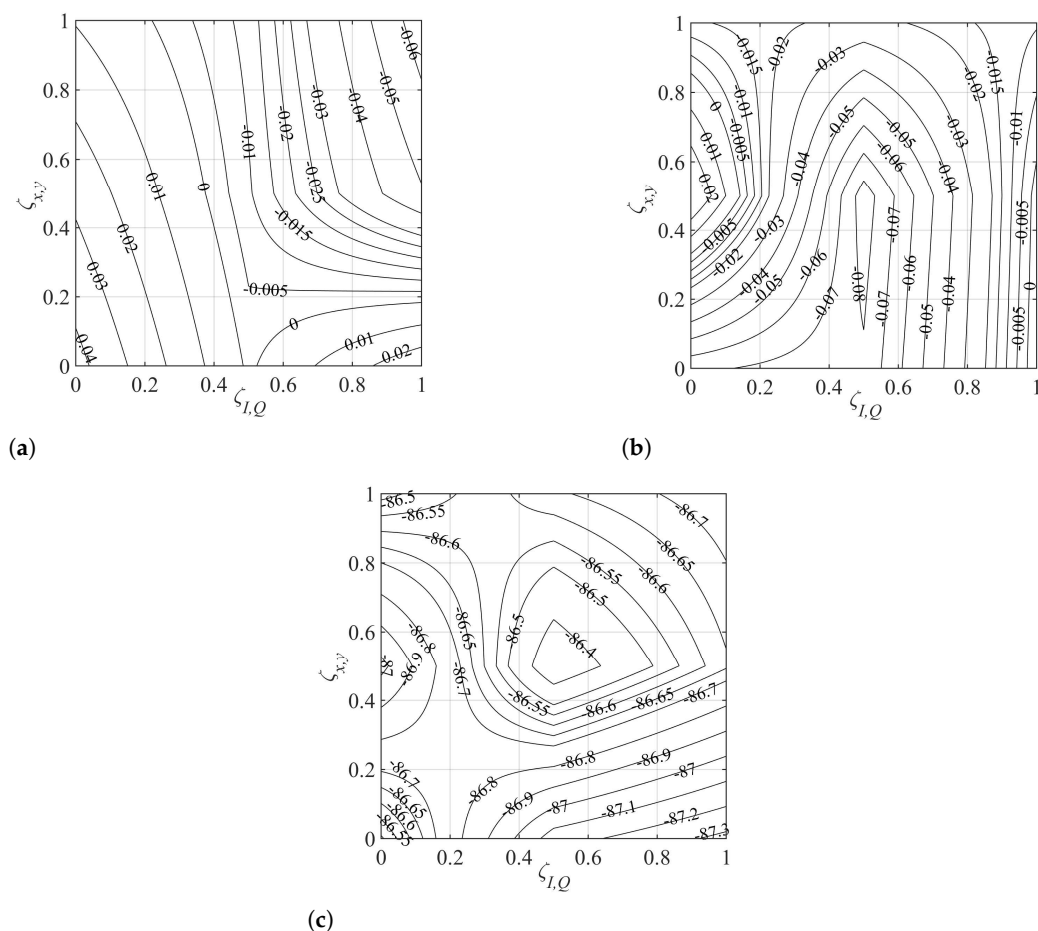


Figure 7. (a) Normalized mean of the I component of the ICXT field in the y direction at the interfered core output; (b) correlation coefficient between the I component of the ICXT field in the y direction and the Q component of the ICXT field in the y direction at the interfered core output; and (c) mean power of the I component of the ICXT field in the y direction at the interfered core output (in dB) for quasi-homogeneous WC-MCF ($\Delta\beta_{c,mn} = -701 \text{ rad} \cdot \text{m}^{-1}$) with $L_C = 10 \text{ m}$ and $L_B = 10 \text{ m}$ (regime $L_C \approx L_B$).

In order to analyze the dependence of the power unbalance of the four ICXT field components, $A_{n,p,q}(L)$, for quasi-homogeneous WC-MCF ($\Delta\beta_{c,mn} = -701 \text{ rad} \cdot \text{m}^{-1}$), on the power distribution at the interfering core input assigned to one of the two directions x or y and one of the two quadrature components I or Q , Figure 8 shows the unbalancing parameter U for the three previous pairs of values (L_B, L_C), and $\Delta\beta_{c,mn} = -701 \text{ rad} \cdot \text{m}^{-1}$, as a function of $(\zeta_{x,y}, \zeta_{I,Q})$ in the range $0 \leq \zeta_{x,y} \leq 1$ and $0 \leq \zeta_{I,Q} \leq 1$.

Figure 8 shows that values of the U parameter lower than 25% are achieved for all situations tested. Such a low unbalancing level indicates that a quasi-uniform power distribution between the four components of the ICXT field occurs for quasi-homogeneous WC-MCF regardless of the power distribution among the four field components at the interfering core input.

We emphasize that the small variations of the normalized mean results around 0 shown in Figures 3a–5a and Figure 7a would be further reduced by increasing the number of simulated samples to a number higher than 200. The same argument holds relating the reduction of the slight variations observed in the mean ICXT power results shown in Figures 3c–5c and Figure 7c as well as relating the reduction of the unbalancing factors shown in Figures 6 and 8. We attribute the nonuniformity of the power distribution between the four components of the ICXT field and the small variations in the normalized mean to the finite number of samples considered in the estimation of the mean power of each ICXT field component from the numerical simulation. An increase in the number

of simulated samples reduces the variance in the corresponding estimators. The small variations around 0 of the correlation results shown in Figures 3b–5b and Figure 7b would be reduced by increasing the number of simulated samples (due to the previous indicated reason) as well as by increasing the MCF length to lengths higher than 100 m due to the decorrelation field effect caused by the increase in the birefringence effects. These behaviors have been observed in a few other ICXT estimates obtained from numerical simulations with up to 500 samples and for WC-MCF lengths of up to 1000 m.

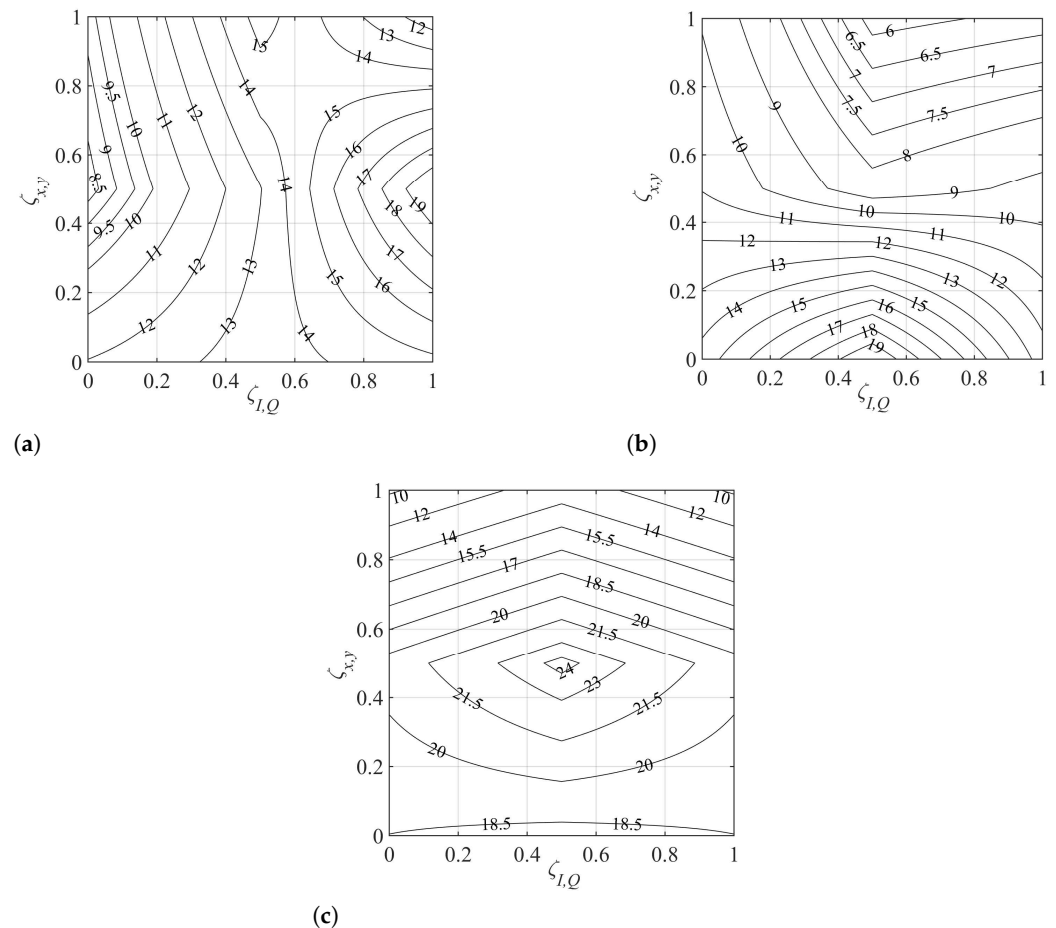


Figure 8. Unbalancing parameter for different pairs (L_B, L_C) and quasi-homogeneous WC-MCF ($\Delta\beta_{c,mm} = -701 \text{ rad} \cdot \text{m}^{-1}$): (a) $L_B = 10$ m, $L_C = 10$ m, (b) $L_B = 10$ m, $L_C = 1$ m, and (c) $L_B = 0.1$ m, $L_C = 10$ m.

6. Conclusions

We assessed by intensive numerical simulation the mean, correlation, and power distribution of the ICXT field components of unmodulated polarization-coupled homogeneous and quasi-homogeneous single-mode WC-MCFs with a single interfering core considering three regimes: (i) $L_C \approx L_B$, (ii) $L_C \ll L_B$, and (iii) $L_C \gg L_B$. For that, the CME model described in Reference [23] to assess the ICXT in a single-mode WC-MCF with intracore birefringence and linear propagation along the longitudinal coordinate of the MCF was used.

We have found that, as it has been reported elsewhere for scalar-coupled single-mode WC-MCFs, the normalized mean of the four ICXT field components and their correlations are very small, with a nearly uniform distribution of the mean power between the four ICXT field components and a very weak dependence on the power distribution of the four field components at the interfering core input. These conclusions were drawn for homogeneous and quasi-homogeneous single-mode WC-MCFs, with birefringence correlation length and birefringence beat length in the ranges of $[0.5 \text{ m}, 10 \text{ m}]$ and $[0.1 \text{ m}, 10 \text{ m}]$, respectively.

These results suggest that, for the range of birefringence correlation length and birefringence beat length typically found in singlecore telecommunication fibers, we may model the ICXT power fluctuations by a χ^2 distribution with four degrees of freedom in homogeneous and quasi-homogeneous polarization-coupled single-mode WC-MCFs, regardless of the distribution of power between the four field components at the interfering core input.

Author Contributions: Conceptualization, A.V.T.C.; methodology, A.V.T.C. and J.A.P.M.; software, J.A.P.M.; validation, A.V.T.C. and J.A.P.M.; formal analysis, A.V.T.C.; investigation, A.V.T.C. and J.A.P.M.; resources, A.V.T.C. and J.A.P.M.; data curation, J.A.P.M. and A.V.T.C.; writing—original draft preparation, J.A.P.M. and A.V.T.C.; writing—review and editing, J.A.P.M. and A.V.T.C.; visualization, J.A.P.M. and A.V.T.C.; supervision, A.V.T.C.; project administration, A.V.T.C.; funding acquisition, J.A.P.M. and A.V.T.C. All authors have read and agreed to the published version of the manuscript.

Funding: This research was partially funded by FCT/MCTES through national funds and, when applicable, co-funded EU funds under the project UIDB/EEA/50008/2020 and project DigCore/UIDP/50008/2020.

Institutional Review Board Statement: Not applicable.

Informed Consent Statement: Not applicable.

Conflicts of Interest: The authors declare no conflict of interest.

Abbreviations

The following abbreviations are used in this manuscript:

CME	Coupled mode equations
CPU	Central processing unit
ICXT	Intercore crosstalk
MCF	Multicore fiber
OCS	Optical communication systems
PC	Personal computer
PDF	Probability density function
RAM	Random access memory
RMM	Random modulus model
WC	Weakly coupled

References

1. Sano, A.; Takara, H.; Kobayashi, T.; Miyamoto, Y. Crosstalk-managed high capacity long haul multicore fiber transmission with propagation-direction interleaving. *J. Lightw. Technol.* **2014**, *32*, 2771–2779. [[CrossRef](#)]
2. Sakaguchi, J.; Puttnam, B.; Klaus, W.; Awaji, Y.; Wada, N.; Kanno, A.; Kawanishi, T.; Imamura, K.; Inaba, H.; Mukasa, K.; et al. 305 Tb/s space division multiple transmission using homogeneous 19-core fiber. *J. Lightw. Technol.* **2013**, *31*, 7554–7562. [[CrossRef](#)]
3. Puttnam, B.; Luís, R.; Agrell, E.; Rademacher, G.; Sakaguchi, J.; Klaus, W.; Saridis, G.; Awaji, Y.; Wada, N. High capacity transmission systems using homogeneous multi-core fibers. *J. Lightw. Technol.* **2017**, *35*, 1157–1167. [[CrossRef](#)]
4. Klaus, W.; Puttnam, B.J.; Luis, R.S.; Sakaguchi, J.; Mendinueta, J.D.; Awaji, Y.; Wada, N. Advanced space division multiplexing technologies for optical networks. *IEEE/OSA J. Opt. Commun. Netw.* **2017**, *9*, C1–C11. [[CrossRef](#)]
5. Li, M.J.; Hayashi, T. Chapter 1—Advances in low-loss, large-area, and multicore fibers. In *Optical Fiber Telecommunications VII*; Willner, A.E., Ed.; Academic Press: Kolkata, India, 2020; pp. 3–50. [[CrossRef](#)]
6. Tsuritani, T.; Soma, D.; Wakayama, Y.; Miyagawa, Y.; Takahashi, M.; Morita, I.; Maeda, K.; Kawasaki, K.; Matsuura, T.; Tsukamoto, M.; et al. Field test of installed high-density optical fiber cable with multi-core fibers toward practical deployment. In *Optical Fiber Communication Conference (OFC) 2019*; Optical Society of America: San Diego, CA, USA, 3–7 March 2019; p. M3J.4. [[CrossRef](#)]
7. Hayashi, T.; Nagashima, T.; Muramoto, T.; Sato, F.; Nakanishi, T. Spatial mode dispersion suppressed randomly-coupled multi-core fiber in straightened loose-tube cable. In *Optical Fiber Communication Conference Postdeadline Papers 2019*; Optical Society of America: San Diego, CA, USA, 3–7 March 2019; p. Th4A.2. [[CrossRef](#)]
8. Hayashi, T.; Nagashima, T.; Nakanishi, T.; Morishima, T.; Kawawada, R.; Mecozzi, A.; Antonelli, C. Field-deployed multi-core fiber testbed. In Proceedings of the 2019 24th OptoElectronics and Communications Conference (OECC) and 2019 International Conference on Photonics in Switching and Computing (PSC), Fukuoka, Japan, 7–11 July 2019; pp. 1–3. [[CrossRef](#)]
9. Fini, J.; Zhu, B.; Taunay, T.; Yan, M. Statistics of crosstalk in bent multicore fibers. *Opt. Express* **2010**, *18*, 15122–15129. [[CrossRef](#)]
10. Takenaga, K.; Arakawa, Y.; Tanigawa, S.; Guan, N.; Matsuo, S.; Saitoh, K.; Koshihara, M. An investigation on crosstalk in multi-core fibers by introducing random fluctuation along longitudinal direction. *IEICE Trans. Commun.* **2011**, *94-B*, 409–416. [[CrossRef](#)]

11. Hayashi, T.; Taru, T.; Shimakawa, O.; Sasaki, T.; Sasaoka, E. Design and fabrication of ultra-low crosstalk and low-loss multi-core fiber. *Opt. Express* **2011**, *19*, 16576–16592. [[CrossRef](#)]
12. Koshihara, M.; Saitoh, K.; Takenaga, K.; Matsuo, S. Multi-core fiber design and analysis: coupled-mode theory and coupled-power theory. *Opt. Express* **2011**, *19*, B102–B111. [[CrossRef](#)]
13. Koshihara, M.; Saitoh, K.; Takenaga, K.; Matsuo, S. Analytical expression of average power-coupling coefficients for estimating intercore crosstalk in multicore fibers. *IEEE Photonics J.* **2012**, *4*, 1987–1995. [[CrossRef](#)]
14. Hayashi, T.; Chen, H.; Fontaine, N.; Nagashima, T.; Ryf, R.; Essiambre, R.; Taru, T. Effects of core count/layout and twisting condition on spatial mode dispersion in coupled multi-core fibers. In Proceedings of the 42nd European Conference on Optical Communication, ECOC 2016, Düsseldorf, Germany, 18–22 September 2016; pp. 1–3.
15. Fujisawa, T.; Amma, Y.; Sasaki, Y.; Matsuo, S.; Aikawa, K.; Saitoh, K.; Koshihara, M. Crosstalk analysis of heterogeneous multicore fibers using coupled-mode theory. *IEEE Photonics J.* **2017**, *9*, 1–8. [[CrossRef](#)]
16. Cartaxo, A.; Alves, T. Discrete changes model of inter-core crosstalk of real homogeneous multi-core fibers. *J. Lightw. Technol.* **2017**, *35*, 2398–2408. [[CrossRef](#)]
17. Soeiro, R.; Alves, T.; Cartaxo, A. Dual polarization discrete changes model of inter-core crosstalk in multi-core fibers. *IEEE Photonics Technol. Lett.* **2017**, *29*, 1395–1398. [[CrossRef](#)]
18. Cartaxo, A.; Morgado, J. New expression for evaluating the mean crosstalk power in weakly-coupled multi-core fibers. *J. Lightw. Technol.* **2021**, *39*, 1830–1842. [[CrossRef](#)]
19. Alves, T.; Soeiro, R.; Cartaxo, A. Probability distribution of intercore crosstalk in weakly coupled MCFs with multiple interferers. *IEEE Photon. Technol. Lett.* **2019**, *31*, 651–654. [[CrossRef](#)]
20. Alves, T.; Cartaxo, A.; Rebola, J. Stochastic properties and outage in crosstalk-impaired OOK-DD weakly-coupled MCF applications with low and high skew×bit-rate. *IEEE J. Sel. Top. Quantum Electron.* **2020**, *26*, 1–8. [[CrossRef](#)]
21. Rebola, J.; Alves, T.; Cartaxo, A. Outage probability due to intercore crosstalk from multiple cores in short-reach networks. *IEEE Photonics Technol. Lett.* **2021**, *33*, 281–284. [[CrossRef](#)]
22. Pinheiro, B.; Rebola, J.; Cartaxo, A. Analysis of inter-core crosstalk in weakly-coupled multi-core fiber coherent systems. *J. Lightw. Technol.* **2021**, *39*, 42–54. [[CrossRef](#)]
23. Antonelli, C.; Riccardi, G.; Hayashi, T.; Mecozzi, A. Role of polarization-mode coupling in the crosstalk between cores of weakly-coupled multi-core fibers. *Opt. Express* **2020**, *28*, 12847–12861. [[CrossRef](#)]
24. Antonelli, C.; Mecozzi, A.; Shtaf, M.; Winzer, P. Random coupling between groups of degenerate fiber modes in mode multiplexed transmission. *Opt. Express* **2013**, *21*, 9484–9490. [[CrossRef](#)]
25. Macho, A.; Garcia-Meca, C.; Fraile-Peláez, F.; Morant, M.; Llorente, R. Birefringence effects in multi-core fiber: Coupled local-mode theory. *Opt. Express* **2016**, *24*, 21415–21434. [[CrossRef](#)]
26. Antonelli, C.; Hayashi, T.; Mecozzi, A. Random polarization-mode coupling explains inter-core crosstalk in uncoupled multi-core fibers. In Proceedings of the 2020 European Conference on Optical Communications (ECOC), Brussels, Belgium, 6–10 December 2020; pp. 1–4. [[CrossRef](#)]
27. Luís, R.; Puttnam, B.; Cartaxo, A.; Klaus, W.; Delgado-Mendinueta, J.; Awaji, Y.; Wada, N.; Nakanishi, T.; Hayashi, T.; Sasaki, T. Time and modulation frequency dependence of crosstalk in homogeneous multi-core fibers. *J. Lightw. Technol.* **2016**, *34*, 441–447. [[CrossRef](#)]
28. Soeiro, R.; Alves, T.; Cartaxo, A. Inter-core crosstalk in weakly coupled MCFs with arbitrary core layout and the effect of bending and twisting on the coupling coefficient. *Opt. Express* **2019**, *27*, 74–91. [[CrossRef](#)] [[PubMed](#)]
29. Amma, Y.; Sasaki, Y.; Takenaga, K.; Matsuo, S.; Tu, J.; Saitoh, K.; Koshihara, M.; Morioka, T.; Miyamoto, Y. High-density multicore fiber with heterogeneous core arrangement. In Proceedings of the 2015 Optical Fiber Communications Conference and Exhibition (OFC), Los Angeles, CA, USA, 22–26 March 2015; pp. 1–3. [[CrossRef](#)]
30. Tu, J.; Saitoh, K.; Koshihara, M.; Takenaga, K.; Matsuo, S. Design and analysis of large-effective-area heterogeneous trench-assisted multi-core fiber. *Opt. Express* **2012**, *20*, 15157–15170. [[CrossRef](#)] [[PubMed](#)]
31. Matsui, T.; Sagae, Y.; Sakamoto, T.; Nakajima, K. Design and applicability of multi-core fibers with standard cladding diameter. *J. Lightw. Technol.* **2020**, *38*, 6065–6070. [[CrossRef](#)]
32. Puttnam, B.; Luís, R.; Klaus, W.; Sakaguchi, J.; Mendinueta, J.D.; Awaji, Y.; Wada, N.; Tamura, Y.; Tetsuya, H.; Hirano, M.; et al. 2.15 Pb/s transmission using a 22 core homogeneous single-mode multi-core fiber and wideband optical comb. In Proceedings of the 2015 European Conference on Optical Communication (ECOC), Valencia, Spain, 27 September–1 October 2015; pp. 1–3. [[CrossRef](#)]
33. Hayashi, T.; Sasaki, T.; Sasaoka, E.; Saitoh, K.; Koshihara, M. Physical interpretation of intercore crosstalk in multicore fiber: effects of macrobend, structure fluctuation, and microbend. *Opt. Express* **2013**, *21*, 5401–5412. [[CrossRef](#)] [[PubMed](#)]
34. Gordon, J.P.; Kogelnik, H. PMD fundamentals: Polarization mode dispersion in optical fibers. *Proc. Natl. Acad. Sci. USA* **2000**, *97*, 4541–4550. [[CrossRef](#)]
35. Galtarossa, A.; Griggio, P.; Palmieri, L.; Pizzinat, A. Low-PMD spun fibers. In *Polarization Mode Dispersion*; Menyuk, C., Galtarossa, A., Eds.; Optical and Fiber Communications Reports (OFCR); Springer Science+Business Media, Inc.: New York, NY, USA, 2005; pp. 246–276. [[CrossRef](#)]
36. Wai, P.K.A.; Menyuk, C.R. Polarization decorrelation in optical fibers with randomly varying birefringence. *Opt. Lett.* **1994**, *19*, 1517–1519. [[CrossRef](#)]

37. Galtarossa, A.; Palmieri, L.; Schiano, M.; Tambosso, T. Measurement of birefringence correlation length in long, single-mode fibers. *Opt. Lett.* **2001**, *26*, 962–964. [[CrossRef](#)]
38. Galtarossa, A.; Palmieri, L.; Pizzinat, A.; Marks, S.; Menyuk, C. An analytical formula for the mean differential group delay of randomly birefringent spun fibers. *J. Lightw. Technol.* **2003**, *21*, 1635–1643. [[CrossRef](#)]
39. Greenside, H.; Helfand, E. Numerical integration of stochastic differential equations-II. *Bell Syst. Technol. J.* **1981**, *60*, 1927–1940. [[CrossRef](#)]
40. Franz, J.; Jain, V. Optical Communications. In *Components and Systems*; Narosa Publishing House: Calcuta, India, 2000.
41. Galtarossa, A.; Palmieri, L.; Schiano, M.; Tambosso, T. Measurements of beat length and perturbation length in long single-mode fibers. *Opt. Lett.* **2000**, *25*, 384–386. [[CrossRef](#)] [[PubMed](#)]
42. Nelson, L.; Jopson, R. Introduction to polarization mode dispersion in optical systems. In *Polarization Mode Dispersion*; Menyuk, C., Galtarossa, A., Eds.; Optical and Fiber Communications Reports (OFCR); Springer Science+Business Media, Inc.: New York, NY, USA, 2005; pp. 1–33. [[CrossRef](#)]
43. Papoulis, A. *Probability, Random Variables, and Stochastic Processes*; Communications and Signal Processing; McGraw-Hill: Singapore, 1991.